

24 1. Introduction

25 Corrosion causes millions of dollars of damage in steel reinforced concrete structures every year. The
26 service life of such structure is critically affected without adequate corrosion protection, especially in
27 harsh environments such as the coastal zones in Australia. Therefore, alternative construction materials
28 were investigated to reduce the cost and maintenance of the structure. Geopolymer concrete (GPC) was
29 considered to have better chloride and sulphate resistance than the Ordinary Portland Cement (OPC)
30 concrete [1,2]. The GPC relies on the formation of an amorphous polymeric Si-O-Al framework instead
31 of the calcium-silicate-hydrates (C-S-H) and calcium hydroxides (C-H) found in OPC matrix. The lack
32 of C-H is advantageous as it actively reacts with the chlorides and sulphates, which in turn reduces the
33 alkalinity in the matrix. The improved chemical stability means that the GPC will continuously provide
34 protection to the embedded reinforcement, extending the service life of the structure. Due to the
35 difference in microstructure, GPC has a lower elastic modulus than OPC concrete [3].

36 Glass Fibre-Reinforced Polymer (GFRP) is also gaining popularity due to its excellent corrosion
37 resistance and high tensile strength. Unlike steel, the GFRP bars do not yield and could be assumed to
38 possess a linear elastic behaviour until failure [4]. GFRP bars have a much lower elastic modulus than
39 steel, therefore they are more susceptible to buckling in compression [5]. Therefore, the unrestrained
40 distance should be reduced by decreasing the spacing of the transverse reinforcement, such as spirals,
41 hoops or stirrups. The short spacing also increased the overall stiffness of the transverse reinforcement,
42 delaying rupturing failures. It was found that by increasing the transverse reinforcement ratio, the load
43 capacity of the members significantly increased [6,7], which demonstrated the contribution of
44 longitudinal GFRP bars in compression. However, international GFRP-reinforced concrete design
45 standards such as ACI 440.1-R15 [8] and CAN/CSA S806-12 [9] do not recommend the inclusion of
46 GFRP bars in the load capacity of the members in compression. Therefore, a better understanding is
47 required for more efficient designs using GFRP.

48 As the concrete continues to rise in compressive strength and reduce in ductility, the ability to predict
49 the load-displacement curves becomes increasingly important. Analytical models were developed for
50 steel-reinforced OPC systems to predict the behaviour under load and determine its ductility. This

51 requirement becomes more apparent for GFRP-reinforced members due to GFRP's inability to yield.
52 For steel-reinforced OPC systems, a handful of analytical models were available. Various confinement
53 models were proposed for axially loaded reinforcement concrete columns. Mander et al. [10] proposed
54 a set of formulations for square, rectangular and circular reinforcement arrangements, which was widely
55 accepted by the research community. However, the opinions on the stress-strain relationship of the
56 eccentrically loaded columns were divided into a few main categories [11]. The first group considered
57 the same stress-strain relationship could be used for both concentrically and eccentrically loaded
58 columns [12,13]. Alternatively, it was believed that a separate stress-strain model must be proposed for
59 eccentrically loaded columns due to the flexural loading [14,15]. The strain-gradient had an influence
60 on the stress distribution in the concrete section, thus affecting the load capacity and ductility of the
61 member. The confinement level varied in each strip of concrete in the cross-section, resulting in a
62 distinct stress-strain relationship. This could be simplified by establishing a model that incorporates the
63 strain gradient effect. Ho and Peng [16] proposed a set of empirical equations for the inverted T-shaped
64 specimens and found good agreements between experimental and predicted results. Feng and Ding [17]
65 introduced the concept of equivalent confinement volume to Mander's model and found that the
66 analytical results matched experimental results closely.

67 A number of research works reported on the behaviour of concentrically or eccentrically loaded GPC
68 or OPC concrete columns fully reinforced with GFRP bars and stirrups. The contribution of longitudinal
69 GFRP bars to the column load carrying capacity varied from 3% to 11% [5,18–21]. The variability was
70 mainly attributed to the amount of transverse reinforcement. For example, the axially loaded column
71 with 75 mm stirrup spacing had a 13.7% and 30.4% higher load carrying capacity than that with a 150
72 mm and 250 mm stirrup spacing, respectively [5]. Additionally, a high transverse reinforcement ratio
73 improved the ductility of the columns and prevented catastrophic brittle failures [5,7]. Overall, GFRP-
74 reinforced columns were more susceptible to slenderness effects than steel due to the lower modulus of
75 GFRP [22]. It was recommended to adopt a slenderness limit of 17 instead of 22 for steel [22]. The
76 main difference between GPC and OPC concrete was that GPC columns had reduced moment
77 capacities, especially when loaded at high eccentricities [7], due to its smaller rectangular stress block

78 [23]. Despite of the distinct behaviour of GFRP-GPC systems from steel-OPC concrete systems, no
79 analytical analysis was carried out for GFRP-reinforced GPC or OPC concrete columns.

80 The literature review highlighted the lack of analytical models for GFRP-reinforced GPC systems. In
81 this study, an analytical model based on flexural analysis was proposed for GFRP-reinforced GPC
82 columns under concentric or eccentric loading. The model was established on the existing principles
83 for modelling the behaviour of steel-reinforced OPC concrete members. It integrated the effect of strain
84 gradient of the confining pressure produced by the transverse GFRP stirrups. Justifications were made
85 to reflect the differences in concrete and reinforcement types, and the loss of load capacity of the
86 concrete cover after spalling. The coefficient of effectiveness was also adjusted accordingly to suit the
87 particular sections studied in this work. The theoretical results were compared against the experimental
88 results for both GFRP-reinforced GPC and OPC concrete columns reported in the literature [5,24].

89 **2. Experimental setup**

90 An experimental investigation of 9 GFRP-reinforced GPC columns was carried out by Elchalakani et
91 al. [5]. The GPC mix had by mass: 15% binder, 6.5% alkali activator mixed with 6.1% water and 0.1%
92 superplasticiser, 29.4% fine aggregates, and 47.3% coarse aggregates. The equal parts fly ash and
93 ground granulated blast-furnace slag (GGBS) binder allowed the specimens to be cured in ambient
94 conditions. The 28-day compressive strength (f'_c) of the GPC was 26.0 MPa. Three specimens with a
95 stirrup spacing of 75 mm, 150 mm and 250 mm were tested under concentric loading and the other six
96 specimens with a 75 mm or 150 mm stirrup spacing were tested at 25 mm, 50 mm and 75 mm
97 eccentricities (e). The low, medium and high eccentricities were selected to examine the effect of
98 bending moment on load capacities. All the specimens have the same rectangular cross-section of $b \times$
99 $d = 260 \text{ mm} \times 160 \text{ mm}$ and height of $h = 1200 \text{ mm}$. The specimens were fully reinforced by GFRP bars
100 and stirrups. The longitudinal bars were 14 mm in diameter and the 8 mm stirrups were used as
101 transverse reinforcement. A 20 mm concrete cover was selected due to the stronger corrosion resistance
102 of the GFRP [5]. The reinforcement layout **in the columns** is shown in Figure 1.

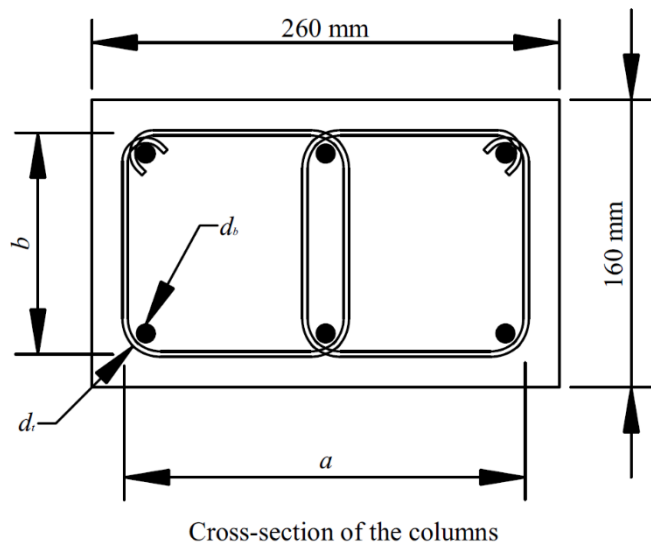
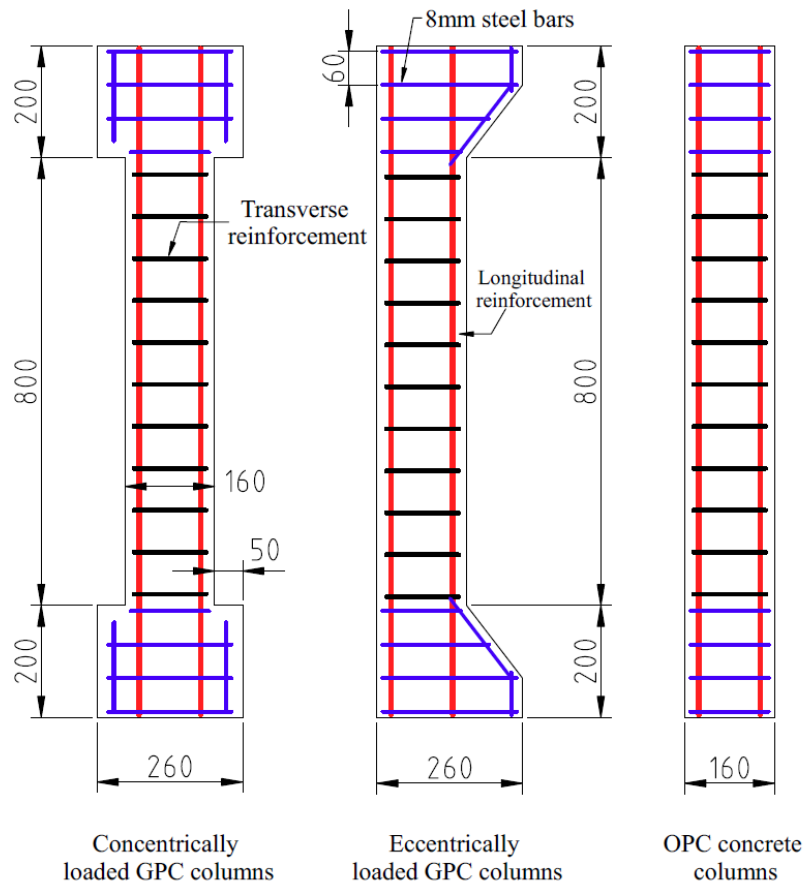


Figure 1. The schematics of the columns

The GFRP-reinforced OPC concrete columns constructed by Elchalakani et al. [24] had a similar cross-section and reinforcement arrangement. A total of 7 GFRP-reinforced columns were tested under

109 concentric and eccentric loading. Another 6 columns were constructed with steel rebars and steel ties.
110 The effect of high load eccentricity was not studied. The f_c of OPC concrete was 32.8 MPa,
111 corresponding to 26.2% higher compressive strength than GPC. The OPC concrete columns were
112 reinforced with 12 mm longitudinal GFRP bars and 6 mm GFRP stirrups. The same 20 mm cover was
113 used in GFRP-reinforced specimens where a 40 mm cover was adopted for steel-reinforced specimens.
114 The specimens in both studies were tested to failure using a universal testing machine with a capacity
115 of 2000 kN. A load-controlled regime was used as the displacement-controlled regime was not available
116 on the machine. A loading rate of 20 kN/min was applied to the column specimens. The eccentricity
117 was provided through a pair of steel rollers welded to the top and bottom end plates of the columns.
118 The rotation about the weaker axis was allowed to ensure that the capacity of the testing machine was
119 sufficient to load the specimens to failure. The specimens were designated in terms of the concrete type
120 (“G” for GPC, “O” for OPC concrete, “S” for steel reinforced OPC concrete), the stirrup spacing in
121 millimetre and the loading condition (“C” for concentric loading, “F” for flexural loading or a number
122 corresponding to the eccentricity in millimetre). For example, “G75-150” represents the GFRP-
123 reinforced GPC column with a 75 mm stirrup spacing loaded at a 150 mm eccentricity. The key design
124 parameters of the specimens tested in the two studies were summarised in Table 1.

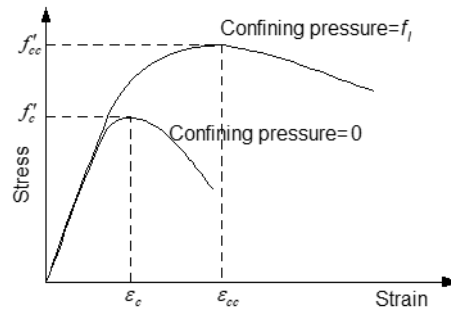
125 **3. Analytical model**

126 The constitutive models used for confined geopolymer concrete, steel and the procedure used in
127 obtaining the load-deformation curves are described in the following sub sections.

128 **3.1 *Proposed stress-strain model for confined geopolymer concrete***

129 The model proposed in this paper was initially developed by the authors for normal and high strength
130 concrete. Further details of the model can be found elsewhere [25]. Two different exponential curves
131 form the complete stress-strain relationships for confined normal strength concrete and geopolymer
132 concrete. The terms described in this constitutive model are shown in Figure 2.

133



134

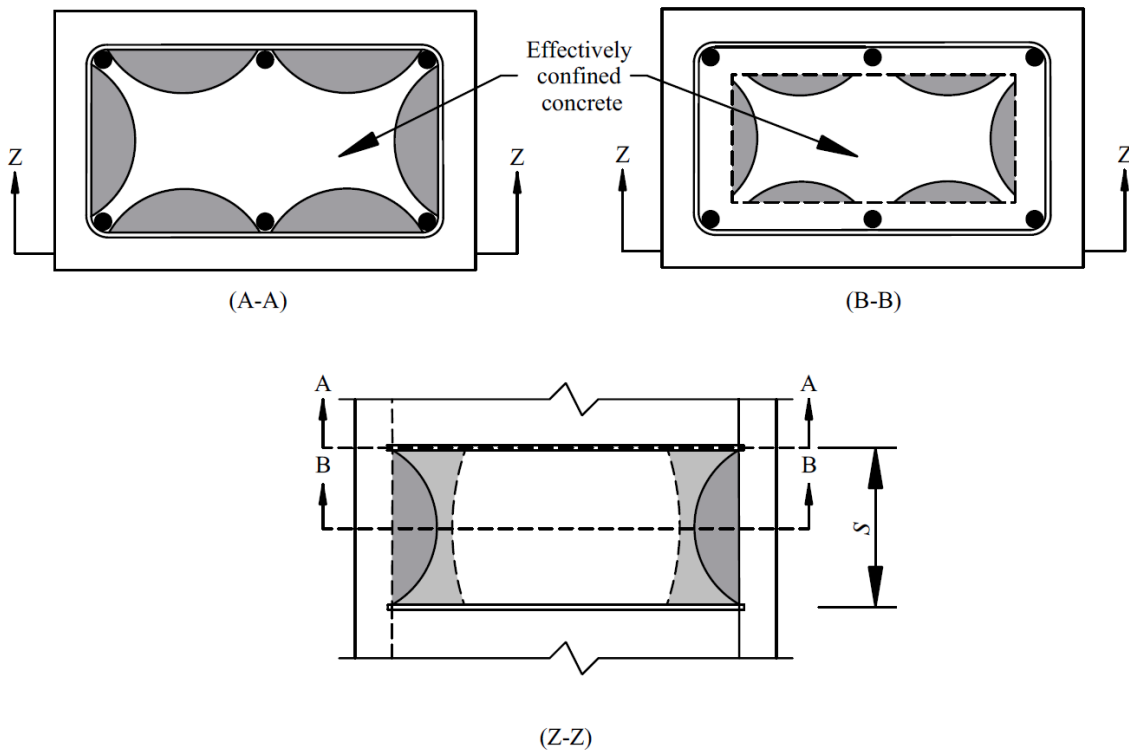
135

Figure 2. Terms used in the stress-strain relationship for geopolymer concrete.

136

137 The uniqueness of this model is that it can predict the lateral deformation as well which can be used to
 138 find the confinement exerted by the confining steel or FRP. The confined region was determined based
 139 on the recommendations by Mander et al. [10], as illustrated in Figure 3. The constitutive model is
 140 briefly described here for the convenience of the reader.

141



142

143

Figure 3. The effectively confined regions

144

145 Axial strain (ε_1) is related to lateral strain (ε_2) as follows:

$$\frac{\varepsilon_2}{\varepsilon'_{cc}} = \begin{cases} \nu_i^a \left(\frac{\varepsilon_1}{\varepsilon_{cc}} \right) & \text{if } \varepsilon_1 \leq \varepsilon' \\ \left(\frac{\varepsilon_1}{\varepsilon_{cc}} \right)^a & \text{if } \varepsilon_1 > \varepsilon' \end{cases} \quad (1)$$

146

147 ε_{cc} and ε'_{cc} are axial and lateral strains corresponding to peak axial stress. Parameter a is a function of
148 the uniaxial concrete strength (f_c) and it is a property of the material. It is given as in Equation 2.

149

$$150 \quad a = 0.0177f_c + 1.2818 \quad (2)$$

151 Equation 1 can be used to find ε' as follows:

$$152 \quad \varepsilon' = \varepsilon_{cc} (\nu_i^a)^{\frac{1}{a-1}} \quad (3)$$

153 The initial Poisson's ratio (ν_i^a) is given as below:

$$\nu_i^a = 8 \times 10^{-6} (f_c)^2 + 0.0002f_c + 0.138 \quad (4)$$

154 Equation 1 completely defines the relationship between axial strain and lateral strain if axial strain (ε_{cc})
155 and lateral strain (ε'_{cc}) corresponding to peak axial stress are known. Axial strain corresponding to peak
156 axial stress ε_{cc} can be expressed as follows.

$$\frac{\varepsilon_{cc}}{\varepsilon_{co}} = 1 + (17 - 0.06f_c) \left(\frac{f_l}{f_c} \right) \quad (5)$$

157 f_l is the confining pressure and ε_{co} is the axial strain corresponding to the peak uniaxial compressive
158 strength. Peak axial stress for confined concrete f_{cc} is defined as:

$$\frac{f_{cc}}{f_c} = \left(\frac{f_l}{f_t} + 1 \right)^k \quad (6)$$

159 where k is a constant given by:

$$k = 1.25 \left(1 + 0.062 \frac{f_l}{f_c} \right) (f_c)^{-0.21} \quad (7)$$

160 f_t is the tensile strength which is given by:

$$f_t = 0.9 \times 0.32 (f_c)^{0.67} \quad (8)$$

161 For a given axial strain, Equations 1-8 can predict the lateral strain if the peak stress and corresponding
 162 lateral strain are known for unconfined concrete strength. The following section describes how to find
 163 the lateral strain corresponding to peak axial stress.

164 Similar to the observations for normal and high strength concrete [25] and for geopolymer paste [26]
 165 it is assumed that geopolymer concrete samples will return to the original volume when the axial strain
 166 is corresponding to the peak axial stress. Therefore, at peak stress:

$$\bar{\varepsilon}_v = \frac{\varepsilon_1 + 2\varepsilon_2}{\varepsilon_{v,\max}} = 0 \quad (9)$$

167

$$\varepsilon_{cc} = 2\varepsilon'_{cc} \quad (10)$$

168 Using the secant value of Poisson's ratio at peak stress (ν_f^a), Equation 10 can be re-written as follows:

$$\nu_f^a = 0.5 \quad (11)$$

169 Using shear stress and shear strain factors, axial stress (σ_1), axial strain (ε_1) and lateral strain (ε_2)
 170 relationships for normal/ geopolymer concrete can be expressed as:

$$\sigma_1 = \begin{cases} 2\tau_{mp} \left(1 - e^{-c \left(\frac{\varepsilon_1 + \varepsilon_2}{2\gamma_{mp}} \right)} \right) + f_l & \text{before peak} \\ 2\tau_{mp} \left(1 - e^{d \left(\frac{\varepsilon_1 + \varepsilon_2}{2\gamma_{mp}} \right)^2 - d} \right) + f_l & \text{after peak} \end{cases} \quad (12)$$

171

172 c and d are material parameters defined as follows:

$$173 \quad c = -0.1f_c + m \quad \text{and} \quad d = -0.0003f_c - 0.0057 \quad (13)$$

174 c is the only material parameter that was modified for normal concrete and geopolymer concrete. m for
175 OPC concrete was used as 5 and that for geopolymer concrete was used as 7.

176 τ_{mp} is the maximum shear stress at peak and γ_{mp} is the corresponding shear strain and are defined in
177 Equation 14.

$$\tau_{mp} = \frac{f_{cc} - f_l}{2} \quad \gamma_{mp} = \frac{\varepsilon_{cc} + \varepsilon'_{cc}}{2} \quad (14)$$

178 Therefore, Equations 1-14 completely define the deformational behaviour of geopolymer concrete.

179 3.2 Stress-strain model for longitudinal bars

180 A simple idealised elasto-plastic stress-strain model was used for steel in this investigation.

$$181 \quad f_s = \begin{cases} E_{st}\varepsilon_s & \text{if } 0 \leq \varepsilon_s \leq \varepsilon_y \\ f_{sy} & \text{if } \varepsilon_s > \varepsilon_y \end{cases} \quad (15)$$

182 where f_s and ε_s are steel stress and strain respectively, E_{st} is the modulus of elasticity and f_{sy} and ε_y are
183 the yield strength and corresponding yield strain of steel.

184 FRP bars are modelled using the below equation.

$$185 \quad f_{frp} = \begin{cases} E_{frp}\varepsilon_{frp} & \text{if } 0 \leq \varepsilon_{frp} \leq \varepsilon_u \\ 0 & \text{if } \varepsilon_{frp} > \varepsilon_u \end{cases} \quad (16)$$

186 where f_{frp} and ε_{frp} are steel stress and strain respectively, E_{frp} is the modulus of elasticity and ε_u is the
187 ultimate strength of FRP bars.

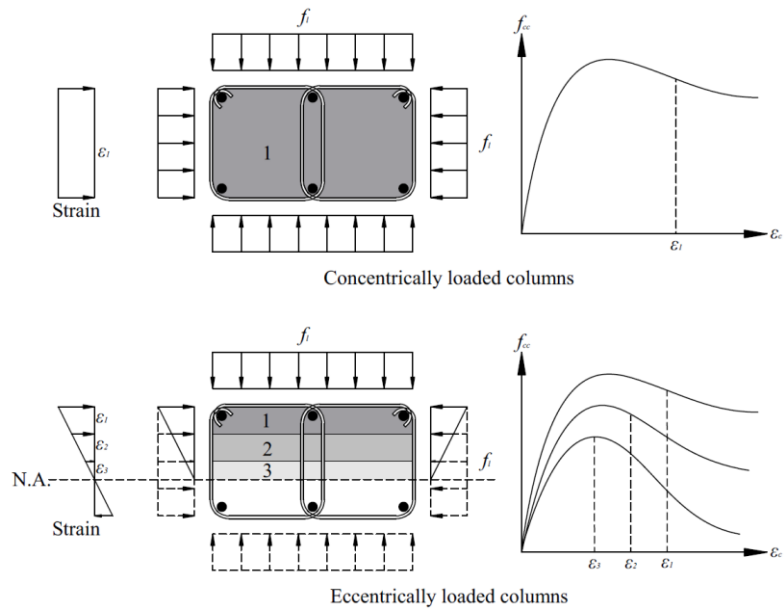
188 3.3 Load-deformation relationships

189 In the analysis process, the section is divided into a number of strips (N). As opposed to concentrically
190 loaded columns, eccentrically loaded columns are subjected to a strain gradient as shown in Figure 4.
191 In order to draw the load deformation curves, a range for the curvature is defined ($\varphi_{initial} = 0$ to φ_{final} in
192 steps of φ_{step}). For an assumed strain distribution (using the given curvature, φ and the assumed strain
193 at extreme compression side, ε_t), strains for each strip as well as for each reinforcement are first
194 determined. Stresses in the core, cover and reinforcement are calculated using the corresponding stress-
195 strain relationships in the previous section. Cover concrete stresses are considered as unconfined
196 concrete stresses while the stresses in reinforcements are obtained using either Equations 15 or 16 for
197 the corresponding strain. For the above assumed strain distribution, the following steps are used to find
198 the stresses in core concrete:

- 199 • Use Equation 1 to find the lateral strain for each of the N number of strips. This is used to find
200 the final lengths for each strip.
- 201 • Deduct the total original lengths of all the N strips (R) from the total final lengths of all the N
202 strips (Q). Use this to find the strain and finally the stress in the stirrup which is used to find
203 the confining pressure provided to the core.
- 204 • Use Equations 1-14 to find the confined concrete stress for each strip in the core.

205 Using all the stresses, forces in core, cover and reinforcement are calculated which are used to find the
206 applied load, the moment and the resulting eccentricity for the assumed strain at extreme compression
207 side, ε_t . For a given curvature, φ and eccentricity, e^* , ε_t is iterated until the calculated eccentricity is
208 equal to the actual eccentricity within a given tolerance level. At this point, calculated load is stored for
209 the corresponding curvature which was used to calculate the deformation. This process is repeated until
210 the curvature reaches φ_{final} . The procedure used in getting the load-deflection curve is shown in Figure
211 5. The analysis process was carried out using a computer program coded in MATLAB.

212

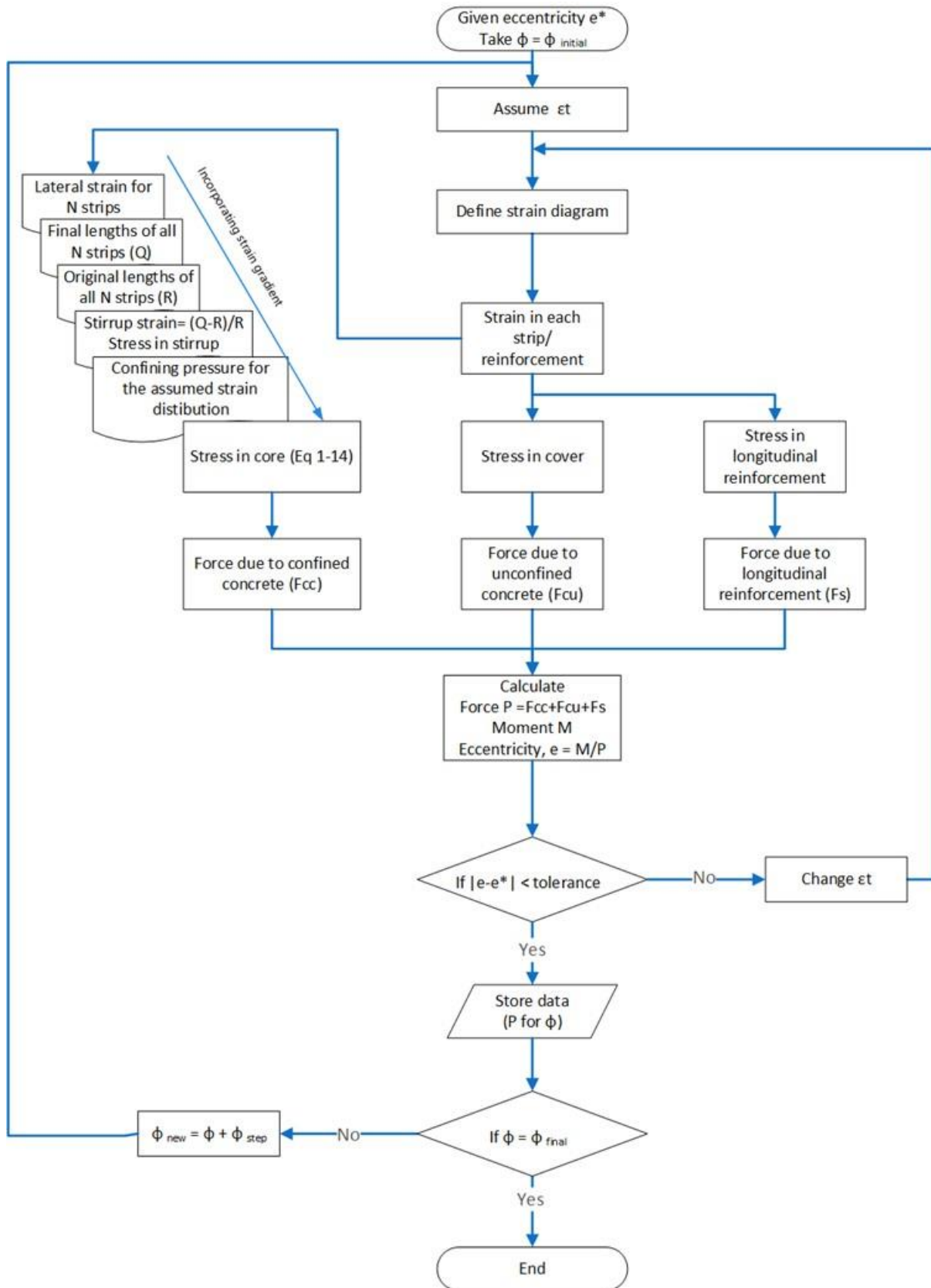


213

214

Figure 4. The strain gradient in the cross-section

215



216

217

Figure 5. Flow chart used to draw load-deflection curves

218

219 4. Comparisons and discussions

220 4.1 *Predicted load and displacement*

221 The experimental and theoretical results are summarised in Table 2. Overall, the theoretical predictions
222 matched well with the experimental results. The predicted loads for GFRP-GPC, GFPR-OPC concrete
223 and steel-OPC concrete all had an average variation of 6% from the experimental data. The variations
224 of the predicted displacements at peak load ranged between 7%-8%. The main discrepancy in the load
225 predictions came from specimens loaded at higher eccentricities. For example, the load capacities of
226 specimen G75-75 and G150-75 loaded at a very high eccentricity of 75 mm were over-predicted by
227 17% and 10%, respectively, whereas their corresponding concentrically loaded columns had a 1% and
228 2% variation, respectively. The over-prediction was less severe in GFRP-OPC concrete and steel-OPC
229 concrete systems. The predicted loads were on average 2% and 5%, respectively, lower than the
230 experimental results, as compared to an average 2% over-prediction for GFRP-GPC systems. It was
231 pointed out that reinforced GPC columns tended to have a reduced rectangular stress block [23].
232 Therefore, as the moment increased in the cross-section, the load capacity was significantly affected.
233 However, the proposed analytical solution was still valid for GFRP-GPC systems. A 97% accuracy was
234 achieved for GFRP-GPC columns loaded at no eccentricity to medium eccentricities. The predicted
235 deflections did not have a clear trend, however a high accuracy of 92% was achieved for all the
236 specimens.

237 4.2 *Predicted ductility*

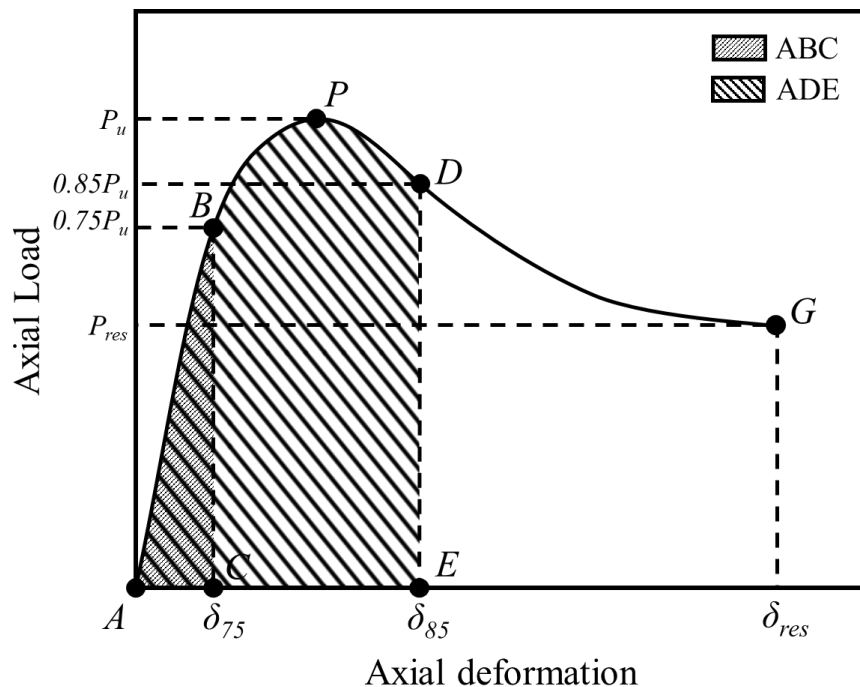
238 As a load-controlled loading regime was adopted for both studies, a special method (Equation 17)
239 proposed in Elchalakani et al. [24] was used to measure the ductility of the columns.

$$240 \quad DI = \frac{ADE}{ABC} \quad (17)$$

241 The ductility index (DI) was a ratio of the work done post peak to the work done in the elastic range.
242 The former was represented by the area ADE under the load-displacement curve, up to the point on the
243 post-peak segment where the load equalled 85% peak load, and the latter was represented by the area

244 ABC up to 75% peak load in the elastic range. The method was illustrated in Figure 6. The DI values
 245 of all the experimental curves and theoretical predictions are reported in Table 2. The ductility of the
 246 GFRP-GPC columns was on average the highest (2.9) among the three groups, followed by GFRP-OPC
 247 concrete columns (2.4) and finally the steel-OPC concrete columns (2.3). It could be seen that a
 248 combination of GFRP bars and GFRP stirrups could improve the ductility over their steel counterpart,
 249 despite that GFRP reinforcement did not yield and have lower stiffness. The columns reinforced with
 250 steel rebars and stirrups were able to reach a higher peak load, however with a reduced ductility. The
 251 steel-reinforced columns had the lowest ductility indices among the three groups, which was likely
 252 attributed to the stiffer response of the steel stirrups. It was reported that the GFRP stirrups gradually
 253 opened up post peak, causing a more steadier loss of capacity observed in specimens such as G75-C [5].
 254 The reason that GPC columns outperformed OPC concrete columns was that the transverse
 255 reinforcement use in the GPC columns was larger in size, which provided better restraint to the
 256 longitudinal bars and better confinement to the concrete.

257



258

259

Figure 6. Ductility index

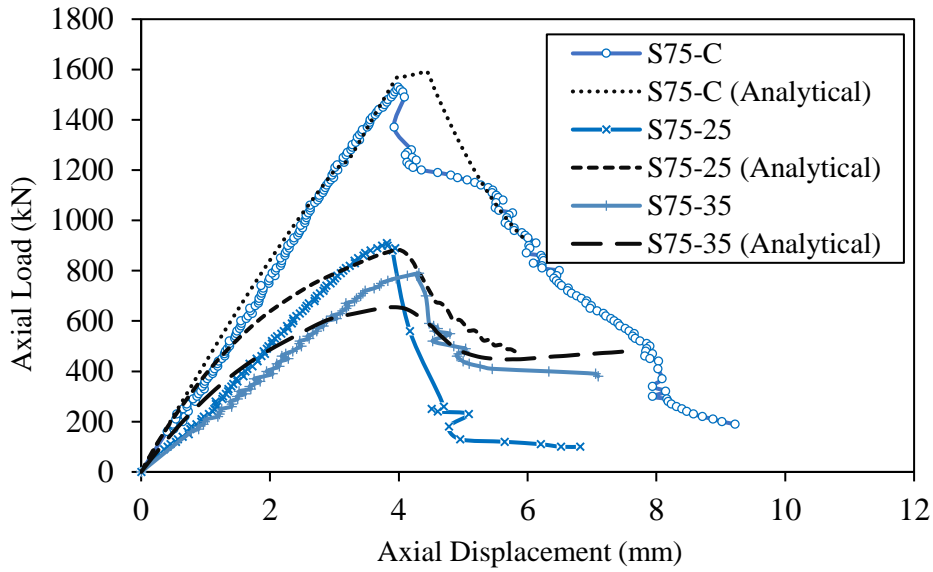
260

261 The analytical results of GFRP-GPC columns were on average the same (2.9) as the experimental
262 results, showing that the model was appropriate for GPC columns. The model tended to slightly over-
263 predict the ductility of GFRP-GPC columns loaded at no or low eccentricities and under-estimate those
264 loaded at higher eccentricities. In comparison, the ductility of all the OPC concrete columns reinforced
265 with steel or GFRP was over-estimated. The average predicted ductility was 3.5 and 2.8 for steel and
266 GFRP reinforced OPC concrete columns, respectively. The reason was likely that a stiffer elastic range
267 was assumed in the analytical model, resulting in a lower ADE value and a greater ductility than tested.
268 The steel-reinforced columns had the lowest ductility indices, similar to the experimental results.

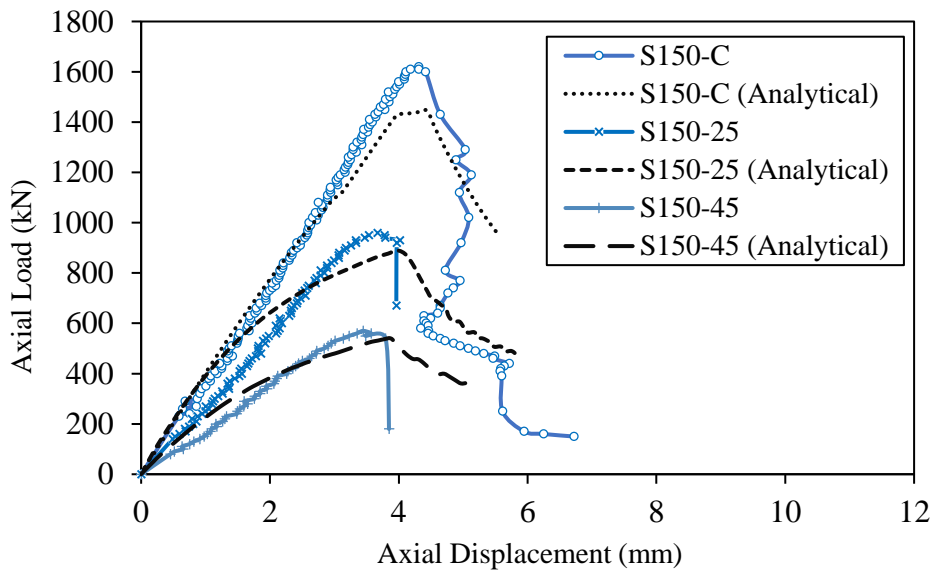
269 **4.3 Steel-reinforced OPC concrete columns**

270 For steel-reinforced columns **as shown in** Figure 7, the analytical model was able to produce accurate
271 peak loads and deflections at peak load. For S75-C, the discrepancy was relatively small and the
272 predicted curve successfully captured the rising and descending segments. However, the predicted
273 elastic range of S75-25 and S75-35 were stiffer than the experimental curves, which resulted in a large
274 predicted ductility. The peak loads of the two columns were slightly under-estimated by the analytical
275 model. A similar trend was observed for those with 150 mm stirrup spacing. The behaviour of the
276 concentrically loaded S150-75 was accurately modelled, however the peak loads of those loaded at an
277 eccentricity were over-estimated. Due to the reduced transverse reinforcement ratio, S150-25 and S150-
278 45 loaded at an eccentricity failed in a more brittle manner. Expectedly, lower residual strengths were
279 seen in the analytical results than the columns with 75 mm stirrup spacing. However, they were still
280 higher than test results, which caused the over-estimation of ductility.

281



282



283

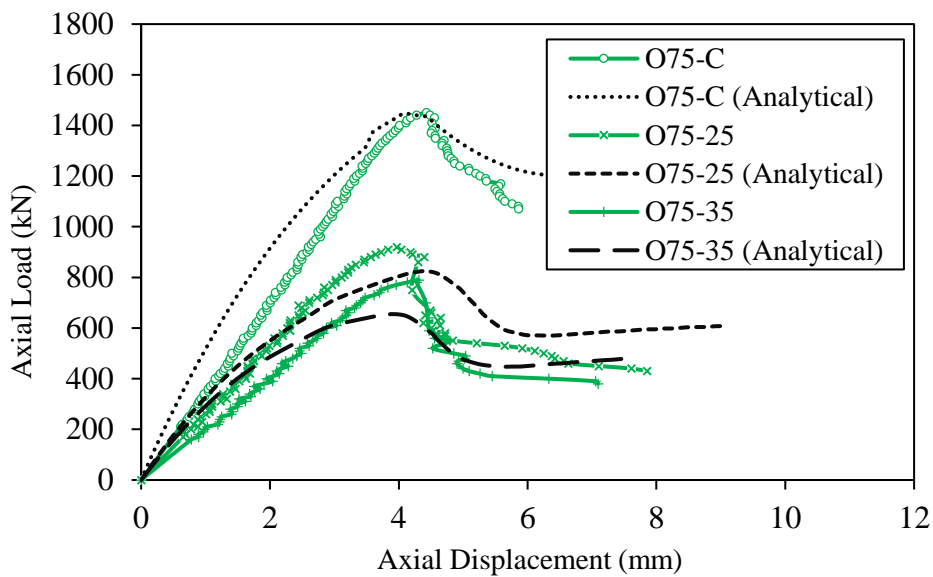
284 Figure 7. Experimental and predicted axial load-axial displacement curves for steel-reinforced OPC
 285 concrete columns

286

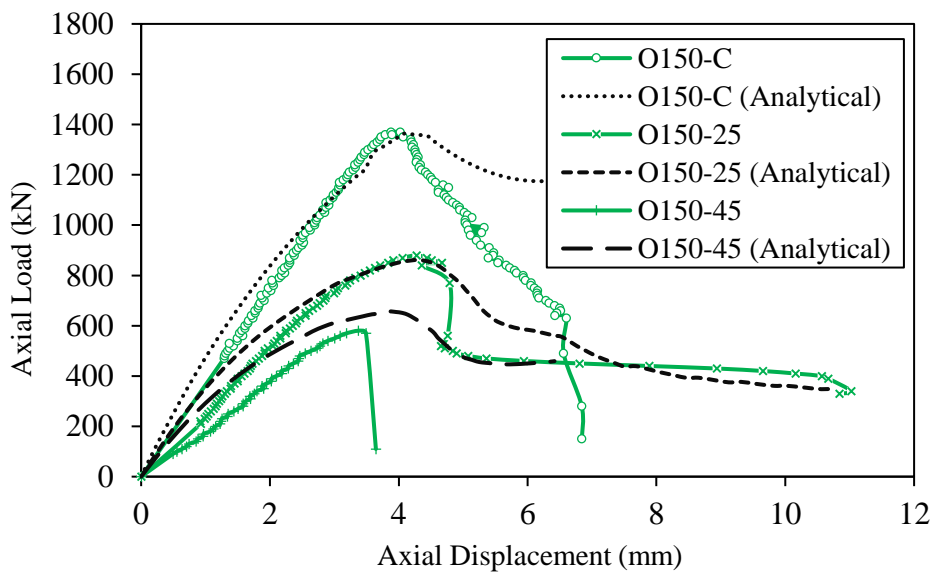
287 **4.4 GFRP-reinforced OPC concrete columns**

288 The behaviour of the GFRP-reinforced OPC concrete columns was generally well captured by the
 289 analytical model. A 6% and 8% variation in peak loads and their corresponding displacements from the
 290 experimental results is observed in Figure 8, respectively. The rising and descending curves of the
 291 concentrically loaded columns from the analytical model were moderately accurate. However, similar

292 to the OPC concrete reinforced with steel rebars and stirrups, the elastic ranges of the eccentrically
 293 loaded columns were stiffer than the test results, resulting in larger ductility indices. The post peak
 294 responses of the columns with 75 mm stirrup spacing were well modelled by the theoretical predictions.
 295 Similar trends were observed for columns with 150 mm stirrup spacing. However, the O150-45 failed
 296 in a brittle manner and was not shown in the predicted curve. In terms of columns with large stirrup
 297 spacings as shown in Figure 9, the predicted behaviour of O250-C also agreed well with the
 298 experimental results, similar to O75-C and O150-C.



299



300

301 Figure 8. The axial load-axial displacement curves of GFRP-reinforced OPC concrete columns

302

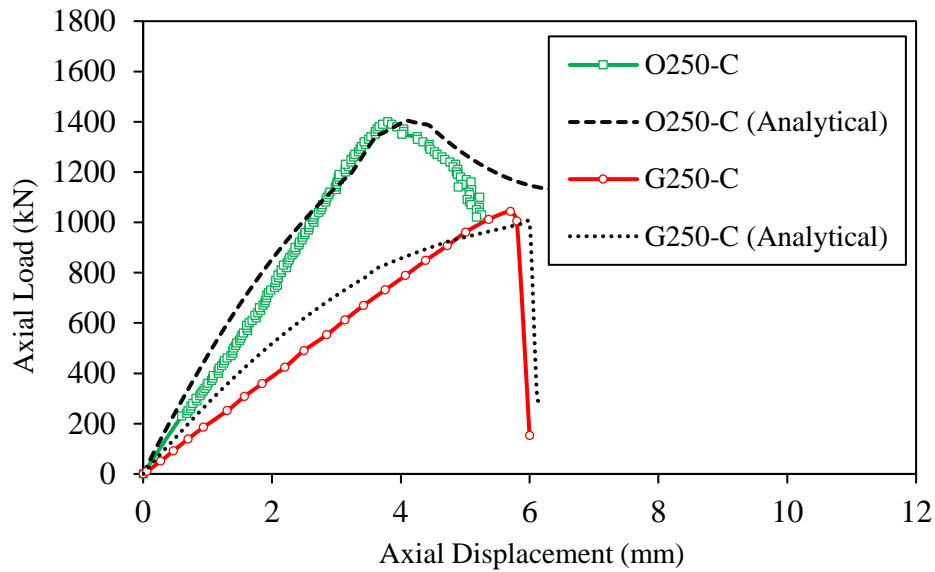


Figure 9. The load-displacement curves of O250-C and G250-C

4.5 GFRP-reinforced geopolymer concrete columns

Figure 10 and 11 show the predicted axial load-axial displacement curves of the GFRP-GPC columns loaded at zero to medium eccentricity (50 mm), and high eccentricity (75 mm), respectively. The GFRP-

GPC columns were most accurately modelled in the elastic ranges and post peak collapse curves.

Therefore, the variations in peak loads, displacements at peak load and ductility indices were satisfactory at 6%, 7% and 18%, respectively. The predicted post peak responses also agreed well with

the experimental behaviour. The elastic range of the G75-C was better captured by the analytical model

than the OPC concrete specimens. As the load eccentricity increased, the inaccuracy of the results

increased. This was attributed to the susceptibility of GPC to bending moment [23]. The height of the

rectangular stress block was smaller than OPC concrete. Despite that, the model was successful in

accurately predicted the behaviour of GFRP-GPC columns loaded at no to medium eccentricity. The

columns with 150 mm stirrup spacing had more brittle responses than those with 75 mm stirrup spacing

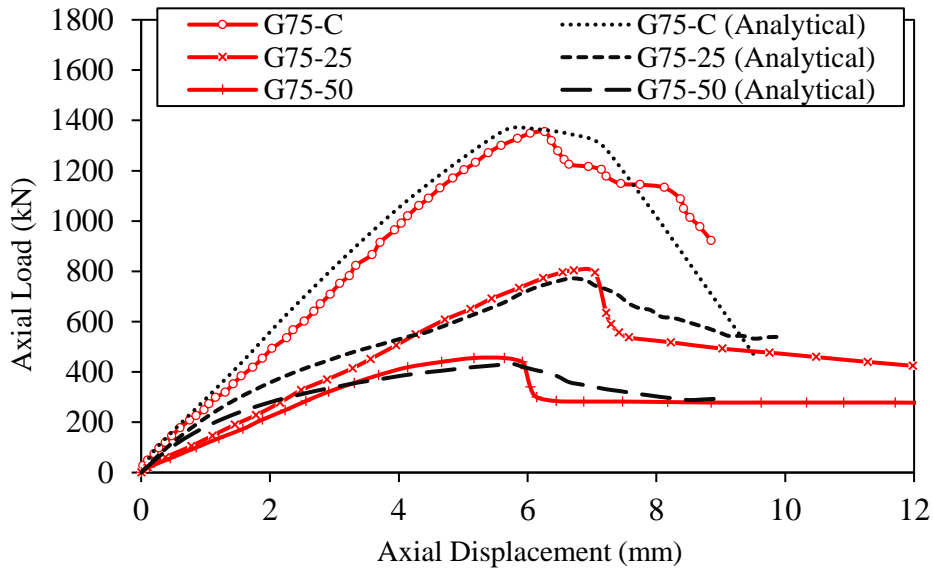
as a result of the less effective transverse reinforcement. This was reflected by the lower *DI* values as

shown in Table 2. The predicted curve of G250-C was amended to Figure 9. From this figure, it could

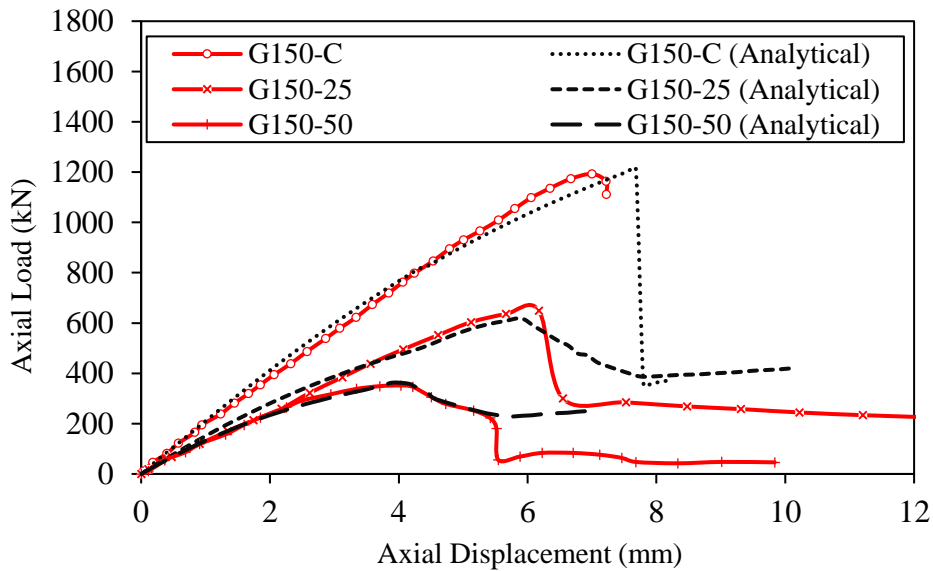
be seen that with a similar geometry and reinforcement arrangement, the GPC columns had a softer

321 elastic range. The post peak response of the GPC column was also more brittle, similar to G150-C.
322 Therefore, sufficient transverse reinforcement must be provided for GPC columns, due to its lower
323 elastic modulus than OPC concrete [3].

324

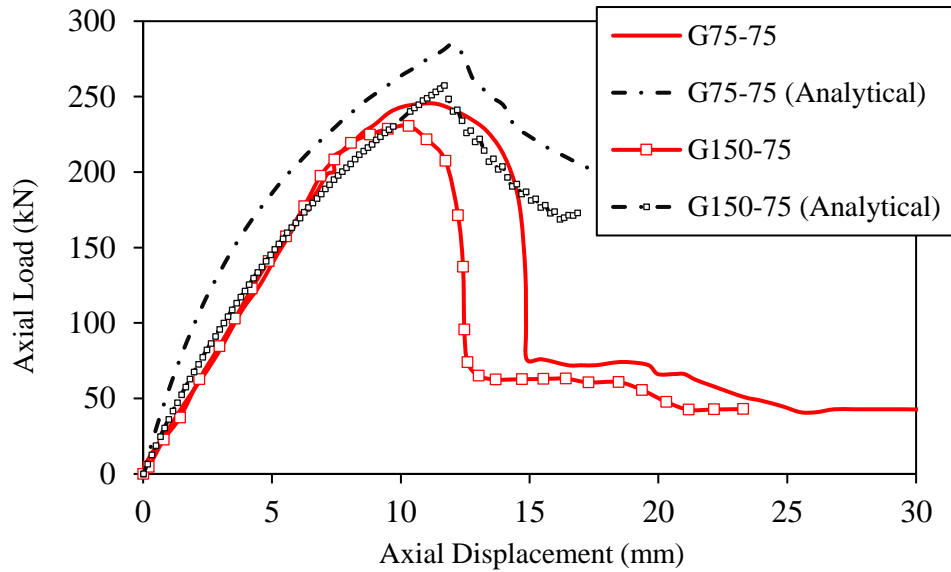


325



326

327 Figure 10. Comparison between analytical and experimental load-deflection curves of the GFRP-
328 reinforced GPC columns



329

330

Figure 11. The axial load-axial displacement curves of G75-75 and G150-75

331

332 5. Conclusions

333 A model was proposed to predict the load-displacement behaviour of the GPC columns fully reinforced
 334 with GFRP bars and stirrups. The model was validated by experimental results, including GFRP-GPC,
 335 GFRP-OPC concrete and steel-OPC concrete columns.

336 It was concluded that model was suitable for modelling the behaviour of the concentrically or
 337 eccentrically loaded GFRP-reinforced GPC columns. On average, the analytical predictions were only
 338 6% and 7% away from the experimental results. The elastic and post peak behaviour could be accurately
 339 predicted up to medium eccentricity ($e/d = 0.31$). As the eccentricity continued to increase, the accuracy
 340 of the model reduced. The proposed model could be applied to the GFRP-reinforced GPC columns.

341 The model was able to produce accurate predictions of GFRP and steel-reinforced OPC concrete
 342 columns. A larger variation of the predicted ductility of GFRP or steel-reinforced OPC concrete
 343 columns was observed. The model tended to over-estimate the stiffness of the OPC concrete columns
 344 in the elastic range, resulting in an over-estimation of the ductility. In comparison, the stiffness of most
 345 GPC columns was accurately modelled in the elastic range.

346 **Acknowledgements**

347 The authors are grateful for the donations and support provided by Pultron Composites, New Zealand
348 and Anthony Miles from Sika Australia.

349 **References**

- 350 [1] Palomo A, Blanco-Varela MT, Granizo ML, Puertas F, Vazquez T, Grutzeck MW. Chemical
351 stability of cementitious materials based on metakaolin. *Cem Concr Res* 1999;29:997–1004.
352 doi:10.1016/S0008-8846(99)00074-5.
- 353 [2] Singh B, Ishwarya G, Gupta M, Bhattacharyya SK. Geopolymer concrete: A review of some
354 recent developments. *Constr Build Mater* 2015;85:78–90.
355 doi:10.1016/j.conbuildmat.2015.03.036.
- 356 [3] Ganesan N, Abraham R, Deepa Raj S, Sasi D. Stress-strain behaviour of confined Geopolymer
357 concrete. *Constr Build Mater* 2014;73:326–31. doi:10.1016/j.conbuildmat.2014.09.092.
- 358 [4] Ibrahim AMA, Fahmy MFM, Wu Z. 3D finite element modeling of bond-controlled behavior
359 of steel and basalt FRP-reinforced concrete square bridge columns under lateral loading.
360 *Compos Struct* 2016;143:33–52. doi:10.1016/j.compstruct.2016.01.014.
- 361 [5] Elchalakani M, Dong M, Karrech A, Li G, Mohamed Ali MS, Yang B. Experimental
362 Investigation of Rectangular Air-Cured Geopolymer Concrete Columns Reinforced with
363 GFRP Bars and Stirrups. *J OfComposites Constr* 2019. doi:10.1061/(ASCE)CC.1943-
364 5614.0000938.
- 365 [6] Hadi M, Karim H, Sheikh N. Experimental investigations on circular concrete columns
366 reinforced with GFRP bars and helices under different loading conditions. *J Compos Constr*
367 2016;20:04016009.
- 368 [7] Elchalakani M, Dong M, Karrech A, Li G, Mohamed Ali MS, Manalo A. Behaviour and
369 design of air cured GFRP-reinforced geopolymer concrete square columns. *Mag Concr Res*
370 2018:1–63. doi:10.1680/jmacr.17.00534.

- 371 [8] ACI 440.1R-15. Guide for the Design and Construction of Concrete Reinforced with FRP
372 Bars. Farmington Hills, MI, USA: American Concrete Institute; 2015.
373 doi:10.1061/40753(171)158.
- 374 [9] CAN/CSA S806-12. Design and Construction of Building Components with Fibre-Reinforced
375 Polymers. Ontario: Canadian Standards Association; 2017.
- 376 [10] Mander JB, Priestley JN, Park R. Theoretical Stress-Strain Model for Confined Concrete. J
377 Struct Eng 1988;114:1804–26.
- 378 [11] Lokuge WP, Setunge ĀS, Sanjayan JGĀ. Modelling eccentrically loaded high-strength
379 concrete columns 2003:331–41. doi:10.1680/mac.55.4.331.37587.
- 380 [12] Eivind Hognestad and Douglas McHenry NWH. Concrete Stress Distribution in Ultimate
381 Strength Design. J Proc 1995;52. doi:10.14359/11609.
- 382 [13] Karsan ID, Jirsa JO. Behaviour of concrete under varying strain gradient. J Struct Eng
383 1970;8:1675–96.
- 384 [14] Sargin M, Ghosh SK, Handa VK. Effects of Lateral Reinforcement upon the Strength and
385 Deformation Properties of Concrete. Mag Concr Res 1971;23:99–110.
- 386 [15] Sheikh SA, Yeh CC. Analytical Moment-Curvature Relations for Tied Concrete Columns. J
387 Struct Eng 2007;118:529–44. doi:10.1061/(asce)0733-9445(1992)118:2(529).
- 388 [16] Ho JCM, Peng J. Strain-Gradient-Dependent Stress-Strain Curve for Normal-Strength
389 Concrete. Adv Struct Eng 2013;16:1911–30. doi:10.1260/1369-4332.16.11.1911.
- 390 [17] Feng D-C, Ding Z-D. A new confined concrete model considering the strain gradient effect for
391 RC columns under eccentric loading. Mag Concr Res 2018;70:1189–204.
392 doi:10.1680/jmacr.18.00040.
- 393 [18] Elchalakani M, Ma G, Aslani F, Duan W. Design of GFRP-reinforced rectangular concrete
394 columns under eccentric axial loading. Mag Concr Res 2017. doi:10.1680/jmacr.16.00437.

- 395 [19] Afifi MZ, Mohamed HM, Benmokrane B. Axial Capacity of Circular Concrete Columns
396 Reinforced with GFRP Bars and Spirals. *J Compos Constr* 2014;18:04013017.
397 doi:10.1061/(ASCE)CC.1943-5614.0000438.
- 398 [20] Tobbi H, Farghaly AS, Benmokrane B. Concrete columns reinforced longitudinally and
399 transversally with glass fiber-reinforced polymer bars. *ACI Struct J* 2012;109:551–8.
400 doi:10.14359/51683874.
- 401 [21] Pantelides CP, Gibbons ME, Reaveley LD. Axial Load Behavior of Concrete Columns
402 Confined with GFRP Spirals. *J Compos Constr* 2013;17:305–13.
403 doi:10.1061/(ASCE)CC.1943-5614.0000357.
- 404 [22] Mirmiran A, Yuan W, Chen X. Design for slenderness in concrete columns internally
405 reinforced with fiber-reinforced polymer bars. *ACI Struct J* 2001;98:116–25.
406 doi:10.14359/10153.
- 407 [23] Tran TT, Pham TM, Hao H. Rectangular Stress-block Parameters for Fly-ash and Slag Based
408 Geopolymer Concrete. *Structures* 2019;19:143–55. doi:10.1016/j.istruc.2019.01.006.
- 409 [24] Elchalakani M, Ma G. Tests of glass fibre reinforced polymer rectangular concrete columns
410 subjected to concentric and eccentric axial loading. *Eng Struct* 2017;151:93–104.
411 doi:10.1016/j.engstruct.2017.08.023.
- 412 [25] Lokuge WP, Sanjayan JG, Setunge S. Stress strain model for laterally confined concrete. *J*
413 *Mater Civ Eng* 2005;17:607–16.
- 414 [26] Haider GM, Sanjayan JG, Ranjith PG. Complete triaxial stress-strain curves for geopolymer.
415 *Constr Build Mater* 2014;69:196–202. doi:10.1016/j.conbuildmat.2014.07.058.